Engineered Science
DOI: https://dx.doi.org/10.30919/es1824

Corrosion-Resistance Properties of Submarine Cable Steel Armor

Guang Yu, Lijie Peng* and Yujia Cheng*

Abstract

In this study, the multifactor coupling corrosion mechanism and the effects of different solutions on the corrosion process were explored in detail. The corrosion of submarine cable steel armor is examined based on the evaluation of the steel corrosion resistance. Here, the research object was hot-dip galvanized steel wire—produced using a continuous galvanizing line—which was then subjected to immersion corrosion experiments. Based on the immersion corrosion experiments and CHI660E electrochemical workstation test, the corrosive effects of a solution containing chloride ions (Cl^-), sulfate ions (SO_4^{2-}), bicarbonate ions (HCO_3^-), and artificial seawater on the hot-dip galvanized steel wire were analyzed in depth. According to the experimental results, the anion species and content influencing corrosion were highest in the artificial seawater. The corrosion rate of the hot-dip galvanized steel wire was fastest in the artificial seawater. However, the corrosion resistance was poor. The corrosion resistance properties of the hot-dip galvanized steel wire in the HCO_3^- solution were the best. In artificial seawater, the effects of the wire corrosion-resistance properties differed considerably, primarily because of the different ionic characteristics. The degree to which the different ions corroded the wire was $SO_4^{2-} > Cl^- > HCO_3^-$. If the salinity increased, the dominant ions influencing corrosion were Cl^- ions—that is, the higher the salinity, the higher the chloride-ion content. The corrosion resistance of steel was poor. At the beginning of the corrosion process, the surface zinc in the hot-dip galvanized steel wire generated an oxidation film, which slowed the corrosion rate, improving the corrosion resistance.

Keywords: Metallographic examination; Corrosion resistance; Hot-dip galvanized steel wire; Electrochemical test.

Received: 24 August 2025; Revised: 03 October 2025; Accepted: 17 October 2025.
Article type: Research article.

1. Introduction

Submarine cable engineering has continually evolved alongside the ongoing development of power transmission technology.[1] Furthermore, submarine cables play key roles in marine energy transmission and communication, providing a vital bond that connects offshore energy production to the land-based power grid.[2] They also facilitate global Internet data transmission.[3]

However, submarine cable construction can be affected by regional construction, marine engineering, and construction equipment conditions.[4] Submarine cables are generally used in complex marine environments for long periods of time and are exposed to seawater corrosion damage, including stress corrosion, chemical corrosion, and seawater microorganism damage.[5] Consequently, steel armor is used as a protective layer for submarine cables.[6] It is self-evident that the steel corrosion resistance is directly related to the service life and operational safety of submarine cables.[7] Currently, the corrosion of submarine cable steel armor as a result of the marine environment is a serious problem.[8] Accordingly, research on improving the corrosion resistance of steel armor should be conducted to ensure the long-term stable operation of submarine cables.[9]

Extensive research vis-à-vis metal corrosion in sea water has been extensively conducted.[10] Here, the corrosion rate and morphology of different steels in seawater environments can be monitored using advanced analog devices designed for marine environments, allowing the corrosion of compound metals in ionic solutions with different chemical compositions to be explored.[11] For example, Zhao *et al*.[12] studied the effect

Mechanical and Electrical Engineering Institute, Zhongshan Institute, University of Electronic Science and Technology of China, Zhongshan 528400, China
* *E-mail*: chengyujia@zsc.edu.cn (Y. Cheng);
15815324196@163.com (L. Peng)

of chloride-ion corrosion on zinc alloys in simulated solutions, as chlorides are a notable cause of corrosion. Additionally, Li *et al*.[13] studied the corrosion behavior of a submarine cable galvanized steel armor under different weak magnetic fields. Using electrochemical corrosion measurements, the effect of magnetic field factors on the corrosion resistance of galvanized steel could be observed. Guo *et al*.[14] focused on the complex galvanic corrosion of galvanized steel and red copper in artificial seawater. The effect of different environmental factors—such as the pH, chloride ions (Cl^-), and dissolved oxygen—on the galvanic corrosion rate was explored. Experimental results showed that galvanic corrosion occurred when galvanized steel and red copper were coupled in a sodium chloride (NaCl) solution. The red copper exhibited a positive electromotive force, and in the NaCl solution, the coupling effect of the galvanized steel increased with H^+ and increasing dissolved oxygen. Kumar and Toor found that the addition of alloying elements was closely related to the steel corrosion resistance.[15] Consequently, multiple marine anticorrosive coating technologies have been developed. Accordingly, Campos *et al*.[16] explored the corrosion behavior of steel armor in an artificial seawater environment based on an immersion test. Research has shown that the corrosion rate decreased gradually over time.

Qiao *et al*.[17] conducted research on hot-dip galvanized steel, focusing primarily on salt-spray-accelerated experimental scenarios. However, the corrosion resistance of hot-dip galvanized steel in Cl^-, sulfate ions (SO_4^{2-}) and bicarbonate ions (HCO_3^-) solutions was less. Deyab and Mohsen studied the corrosion of alloys in different ionic solutions. They were not, however, submarine cable steel armor; furthermore, their study lacked systematic evidence.[18]

In summary, the corrosion behavior of submarine cable steel armor has only been explored in a few respects in current research.[19] Owing to the lack of comprehensive multidimensional studies—such as immersion corrosion tests and electrochemical experiments—the corrosion mechanism of hot-dip galvanized steel in complex marine environments has not been exhaustively explored.[20]

In this study, the corrosion resistance of hot-dip galvanized steel in Cl^-, SO_4^{2-}, and HCO_3^- solutions and artificial seawater was analyzed in depth. The aim was to provide more targeted data for the practical application of submarine cable hot-dip galvanized steel armor. Based on the immersion corrosion tests and electrochemical experiments conducted, the anti-corrosion behavior of hot-dip galvanized steel armor in complex marine environments could be comprehensively examined, revealing the macroscopic corrosion phenomena of hot-dip galvanized steel and its corrosion mechanism at the microlevel. Additionally, the electrochemical reactions during the corrosion process were analyzed in detail, from which the corrosion process of hot-dip galvanized steel could be fully understood. The findings of this study provide a theoretical basis for the development of anti-corrosion measures for submarine cable steel armor.

2. Materials and methods

2.1 Experimental steel selection

All experiments followed industry standards and specifications for marine engineering and power cables. The experimental steel selection conformed to the International Electrotechnical Commission (IEC) standard. Accordingly, the marine cable was required to exhibit the following characteristics:

1) Triaxial cables should generally be selected.
2) The submarine cable steel armor should possess good corrosion resistance.
3) The tensile strength of the submarine cable steel armor should be sufficiently high—that is, between 900–2000 MPa in general.
4) The submarine cable steel armor should possess good flexibility; accordingly, steel wire was used, allowing the submarine cable to bend based on the complex submarine topography and laying process.

Consequently, according to the IEC standard, galvanized steel wire was used as the triaxial cable armor layer. By considering the experimental costs, marine environment, commonly used size, steel flexibility, and tensile strength, the hot-dip galvanized steel wire produced by Ashfaq *et al*.[21] was selected. The diameter of the steel wire was 2.2 mm, as shown in Fig. S1(a) of support information, and the tensile strength was 1370 MPa. The zinc layer on the hot-dip galvanized steel wire surface could effectively separate the seawater from the steel wire matrix. The steel wire was fine and exhibited good flexibility, meeting the demands of the complex submarine topography. The hot-dip galvanized steel was cut into small steel samples with a length of 8 mm and 3 g in weight. Two cross-sections of the steel samples were then sanded until they were smooth. The steel samples were polished using an MC004-MP-2 metallographic grinding and polishing machine, as shown in Fig. S1(b) of support information. The rotational speed was set to 1200 rpm. A polishing paste used in the moderation process was applied before polishing; each polishing process lasted 3 min, and each steel sample was polished 2–3 times. After polishing, the samples were dried. To prevent corrosion, they were stored in a dry and clean environment, the prepared steel samples being as shown in Fig. S1(c) of support information.

2.2 Corrosion solution preparation

The components and content of seawater ions can differ considerably. To accurately simulate real seawater characteristics, nine test solutions were used in this study that satisfied the demands of the different experimental stages.[22]

Artificial seawater: 3.5% salinity, to simulate the components of natural seawater.

Sodium chloride (NaCl) standard solution: 2.30%, 5%, and 10% density.

Sodium sulfate (Na_2SO_4) standard solution: 0.35% and 5% density.

Sodium bicarbonate ($NaHCO_3$) standard solution: 0.02%, 3%, and 5% density.

(1) *Solution for the macroscopic immersion corrosion test*: Seven solutions were selected for the test. Based on the flow-accelerated corrosion (FAC) principles and salt spray tests, the solution concentration was increased appropriately, as listed in Table 1.

Solution ①: Artificial seawater, used to explore the material corrosion morphology and rate under oceanic conditions.

Solutions ② and ⑥: NaCl standard solutions of differing content, used to explore the effect of Cl^- on the material corrosion. The relationship between the solution content and the corrosion degree was determined.

Solutions ③ and ⑤: $NaHCO_3$ standard solutions of differing content, used to explore the effects of the alkaline environment and HCO_3^- on the material corrosion.

Solution ④: 5% Na_2SO_4 standard solution, used to explore the effect of SO_4^{2-} on the material corrosion.

Solution ⑦: Clean water. This was a control group without special ions, used for comparison with the other solutions.

In actual marine or industrial environments, the chloride-ion content differs. Consequently, steel corrosion under chloride-ion enrichment was investigated using a 10% NaCl standard solution. However, the 5% NaCl standard solution was closer to the chloride-ion content of the general marine environment. Subsequently, the effect of different chloride-ion concentrations on the corrosion of steel could be explored. Then, 3% and 5% $NaHCO_3$ standard solutions were used to explore the effect of different alkaline strengths and bicarbonate content on the corrosion resistance of the materials. The alkaline environment and bicarbonate ion content affect the formation, structure, and properties of corrosion products, as well as the corrosion rate and morphology of the materials.

The macroscopic immersion corrosion tests were divided into two experimental groups. In ordinary seawater, the Cl^- content > SO_4^{2-} content > HCO_3^- content. Consequently, Solutions ①, ②, ③, ④ and ⑦ were placed in group one, based on their different seawater ion content. In this group, the effect of different ions and acid-base environments on the corrosion behavior of the materials could be explored. From the experimental observations in this group, the material corrosion phenomenon in a complex chemical environment could be analyzed in multiple dimensions. Solutions ④, ⑤, ⑥, and ⑦ were placed in group two. The ion content of each solution in this group was 5%. The effect of different ions on the corrosion resistance of the materials were explored. This variable was an effective control when the ion concentration was fixed. The intrinsic properties of each ion were also investigated.

(2) *Solution for the microscopic experiments*: In the microscopic experiment, Solution ⑦ differed from the solution in the immersion corrosion macroscopic test. All other solutions were identical, as listed in Table 2. In this experiment, Solution ⑦ was a nitric acid solution (NHO_3) with 4% ion content. After polishing, the steel samples were corroded using the 4% NHO_3 solution. Samples without corrosion were used as the control group, from which the crystal boundaries of the steel samples under normal conditions could be observed. In this experiment, the crystal boundaries of the steel samples were observed before and after corrosion.

(3) *Solution for the electrochemical workstation test*: Here, four solutions were selected for testing. The solution composition was based on the ion content of ordinary seawater, as listed in Table 3.

1) *Sodium chloride solution concentration calculation*: The chloride-ion content in ordinary seawater was 14.1 g/L. The relative atomic mass was 35.5. The relative atomic mass of Na was 23. Consequently, the molar mass of NaCl was 58.5 g/mol. In the 1 L NaCl solution, the NaCl quantity was 14.1/35.5 = 0.397 mol. The NaCl mass was 0.397×58.5 = 23.2 g. At this point, the NaCl mass fraction was 23.2/(1000+23.2)×100% = 2.27%. Therefore, the actual NaCl solution concentration was 2.30%.

2) *Na_2SO_4 solution concentration calculation*: The sulfate ion content in ordinary seawater was 2.25 g/L. The molar masses of the sulfate ions and Na_2SO_4 were 96 and 142 g/mol, respectively. In the 1 L Na_2SO_4 solution, the Na_2SO_4 quantity was 2.25/96 = 0.0234 mol. The Na_2SO_4 mass was 0.0234×142 = 3.32 g. At this point, the Na_2SO_4 mass fraction was 3.32/(1000+3.32)×100% = 0.33%. Therefore, the actual Na_2SO_4 solution was 0.35%.

3) *$NaHCO_3$ solution concentration calculation*: The bicarbonate ion content in ordinary seawater was 0.1478 g/L.

The molar masses of bicarbonate ions and $NaHCO_3$ were 61 and 84 g/mol, respectively. In the 1 L Na_2SO_4 solution, the $NaHCO_3$ quantity was 0.1478/61 = 0.00242 mol. The $NaHCO_3$ mass was 0.00242×84 = 0.203 g. At this point, the $NaHCO_3$ mass fraction was 0.203/(1000+0.203)×100 = 0.02%. Therefore, the actual concentration of the $NaHCO_3$ solution was 0.02%. The different solutions used in the electrochemical test are listed in Table 4.

2.3 Immersion corrosion macroscopic experimental procedure

This experiment was conducted as follows:

1) The seven solutions were poured into 50-mL beakers.

2) Labels were attached to the steel samples. Four samples were placed into each beaker.

3) The original weights of the steel samples were recorded. Additionally, the macroscopic surface state was observed.

4) On days 3, 10, 15, and 20, the macroscopic surface states of the different corrosion samples were observed. The solution conditions were also recorded, including the material release, solution color change, and presence of sediment.

5) All data were processed. The relationships between the solution composition and degree of steel corrosion was examined.

6) The steel corrosion resistance under different solution environments was evaluated based on the test results.

2.4 Micro morphology testing

The micro morphology tests were conducted as follows:

1) Six polished steel samples were prepared. The samples were then washed with absolute alcohol to remove any surface impurities.

2) A 4% nitric acid solution was dripped onto the cross sections of the steel samples. After 8 s of corrosion, the samples were flushed with alcohol. The samples were then dried quickly.

3) The cross-sections of the steel samples were observed using a microscope, from which metallographic images of the original steel samples were recorded. These images were used for contrast-enhanced imaging.

4) The steel samples were subjected to immersion corrosion. During this process, the cross sections of the steel samples did not touch the bottom or walls of the beaker to avoid damage to the cross sections.

5) After 5 min, all steel samples were removed and dried. The metallographic surfaces were observed using a metallurgical microscope. The metallographic structures and grain-boundary changes were recorded.

6) After 24 h immersion, the steel samples were collected and dried. The metallographic surfaces were observed using a metallurgical microscope.

7) Based on observations at different times, the effects of different solutions on the metallographic structure and grain

Table 1: Type and number of immersion corrosion macroscopic test solutions.

Number	①	②	③	④	⑤	⑥	⑦
Solution	Artificial seawater	10% NaCl	3% $NaHCO_3$	5% Na_2SO_4	5% $NaHCO_3$	5% NaCl	Clean water

Table 2: Type and number of microscopic test solutions.

Number	①	②	③	④	⑤	⑥	⑦
Solution	Artificial seawater	10% NaCl	3% $NaHCO_3$	5% Na_2SO_4	5% $NaHCO_3$	5% NaCl	4% NHO_3

Table 3: Ion content in the different solutions.

Ions	Cl^-	SO_4^{2-}	HCO_3^-
Content (mg/L)	1.41×10^4	2.25×10^3	147.8

Table 4: Type and number of the electrochemical test solutions.

Number	①	②	③	④
Solution	Artificial seawater	2.30% NaCl	0.35% Na_2SO_4	0.02% $NaHCO_3$

boundaries were examined, from which the steel corrosion behaviors and products in different solutions could be obtained.

2.5 Electrochemical workstation testing

The electrochemical tests were conducted as follows:

1) The test solution was poured into the tertiary system container.

2) Tertiary system clips were fixed to the counter electrodes. A green clip was attached to the working electrode. Polished steel samples were used as the working electrodes. A white clip was attached to the reference electrode. A red clip was attached to the counter electrode.

3) For testing, the CHI660E electrochemical workstation testing software was used and calibrated.

4) *Open-circuit potential test*: After setting the parameters, the test was initiated. After 30 min of stable operation, the open-circuit potential was measured and recorded.

5) *Resistance test*: The open-circuit potential parameters were used as the initial potential parameters in the resistance test. The maximum and minimum frequency were set to 100,000 and 0.01 Hz, respectively. The voltage amplitude was set to 0.005 V. The other parameters were the default settings of the system.

6) *Polarization curve test*: In the polarization curve parameter settings, an open-circuit potential of +500 mV was set as the final potential. An open-circuit potential of –500 mV was used as the initial potential. The scan rate was set to 0.001 V/s. This test was run in autosensing form.

The test for each solution was repeated at least three times. All data and charts were summarized according to the reference electrode.

3. Results and discussion

3.1 Immersion corrosion test results and analysis

Before immersion corrosion, the sample surfaces were all smooth. All solutions were colorless and had no sediment, as shown in Fig. S2 of support information. As immersion corrosion began, the steel samples were observed on Days 3, 10, 15, and 20. The observations on Days 3, 10, 15, and 20 are presented in Tables 5-8, respectively.

1) *Chloride-ion (Cl^-) solution*: When the NaCl concentration was high, the effect of chloride ions on the hot-dip galvanized steel wire corrosion was strong. A large number of chloride ions weakened the corrosion resistance of the steel considerably. When the steel samples were in the low-concentration chloride solution (5% NaCl), the corrosion degree was lower than that in the 10% solution but higher than that in the artificial seawater. This was because the chloride concentration in the artificial seawater was the lowest.

2) *Bicarbonate ion (HCO_3^-) solution*: The steel samples in the 3% $NaHCO_3$ solution were corroded slowly. Even on Day 20, rust spots were not apparent. Low concentrations of bicarbonate ions and an alkaline environment weakly affected the hot-dip galvanized steel wire corrosion process. The effect of this solution on the steel corrosion resistance was low. In the 5% $NaHCO_3$ solution, the degree of steel corrosion was also mild.

3) *Sulfate ion (SO_4^{2-}) solution*: With the steel samples in the 5% Na_2SO_4 solution, the corrosion rate and degree was lower than that in the chloride-ion solution but higher than that in the bicarbonate-ion solution. Thus, the sulfate ions caused a certain degree of corrosion in the hot-dip galvanized steel wire.

4) *Artificial seawater solution with 3.5% salinity*: This solution contained multiple ions. The test results showed that the marine environment had a major corrosive effect on the hot-dip galvanized steel wire.

5) *Clean water*: In this solution, the hot-dip galvanized steel wire was corroded slightly. Even the protective layer of the zinc coating could not be corroded.

Based on these test results, four main conclusions can be summarized as follows:

1) In artificial seawater environments, the corrosion of submarine cable steel armor should not be ignored. However, in clean water, the test steel was barely corroded.

2) Based on the corrosion of steel samples in solutions with the same ions of different concentrations, the corrosion increased as the ion concentration increased.

3) In the chloride-ion solution, the steel was corroded more severely than in the bicarbonate-ion solution.

4) Based on the corrosion of steel samples in solutions with the same concentrations (5%) and different ions, the steel was seriously corroded in the sulfate- and chloride-ion solutions. According to our preliminary judgment, in seawater, the chloride and sulfate ions affected the corrosion of submarine cable steel armor greatly.

3.2 Metallographic structure microscopic detection

1) Metallographic structure of normal steel: As shown in Fig. 1, the atomic arrangement at the Continuously Galvanizing Line (CGL) low-carbon steel crystal boundary was disordered. The atomic arrangement of the grains was regular. The grains had an irregular polygonal morphology and were tightly arranged. The grain sizes were homogeneous. The grain boundary presented a clear, twisted line that separated the different grains. However, there was no evident coarsening or abnormal thickening of the grain boundaries, indicative of their stable state.

As shown in Fig. 1, the metallographic structure of the

Table 5: Immersion corrosion observations on Day 3.

Solution	Sample surface morphology	Solution state	Corrosion degree	Corrosion resistance
①	A little dark gray material	White dot sediment	Mild	Slight decrease
②	More dark gray material than in Solution ①	A little cloudy	Moderate	A measure of decrease
③	Less dark gray material than in Solution ①	No major changes	Mild	Slight decrease
④	Light blue surface layer adheres to the dark gray material	A little cloudy	Mild	Slight decrease
⑤	Less dark gray material than in Solution ①	No major changes	Mild	Slight decrease
⑥	More dark gray material than in Solution ①	A little cloudy	Mild	Slight decrease
⑦	Small-area light gray oxide layer	No major changes	Very mild	Little influence

Table 6: Immersion corrosion observation on Day 10.

Solution	Sample surface morphology	Solution state	Corrosion degree	Corrosion resistance
①	The area of dark gray material expands	A little cloudy, a little white flocculent precipitate	Moderate	Moderate decrease
②	Surface turns black, zinc layer is destroyed, rust spots exists	Turbidity is high, white precipitate exists	Moderate	Major decrease
③	The area of dark gray material expands	Relatively clear	Mild	Slight decrease
④	Surface turns black, zinc layer has minor damage	Turbidity increases	Moderate	Moderate decrease
⑤	The area of dark gray material expands	Relatively clear	Mild	Slight decrease
⑥	Surface turns black, zinc layer is destroyed	Turbidity increases	Moderate	Moderate decrease
⑦	Area of light gray oxide layer increases	No major changes	Very mild	Little influence

Table 7: Immersion corrosion observation on Day 15.

Solution	Sample surface morphology	Solution state	Corrosion degree	Corrosion resistance
①	Surface turns black, zinc layer is destroyed, rust spots exist	A little cloudy, white precipitant increases	Moderate	Major decrease
②	Zinc layer has moderate damage, rust spot area expands	The solution turns yellow	Severe	Severe decrease
③	The area of dark gray material expands	Tiny amounts of precipitate exist	Moderate	Slight decrease
④	Surface turns black, zinc layer is destroyed, rust spots exist	Turbidity increases, tiny amounts of precipitate exist	Moderate	Major decrease
⑤	Surface turns black	Tiny amounts of precipitate exist	Moderate	Slight decrease
⑥	Zinc layer has moderate damage, rust spots exist	Turbidity increases, Tiny amounts of precipitate exist	Moderate	Major decrease
⑦	Area of gray oxide layer increases	No major changes	Very mild	Little influence

Table 8: Immersion corrosion observation on Day 20.

Solution	Sample surface morphology	Solution state	Corrosion degree	Corrosion resistance
①	The rust spot area expands	The precipitate increases a little	Moderate	Major decrease
②	The rust spot area expands, rust layer thickens	The solution is deep yellow	Severe	Severe decrease
③	A small number of rust spots, the rusted area is small	The precipitate increases a little	Moderate	A measure of decrease
④	The rusted spot area is large	Turbidity increases, the solution is light yellow	Severe	Severe decrease
⑤	A small number of rust spots, the rusted area is small	Tiny amounts of precipitate exist	Moderate	A measure of decrease
⑥	The rust spot area expands, rust layer thickens	Turbidity increases, there is more precipitation	Severe	Severe decrease
⑦	Area of gray oxide layer increases	No major changes	Very mild	Little influence

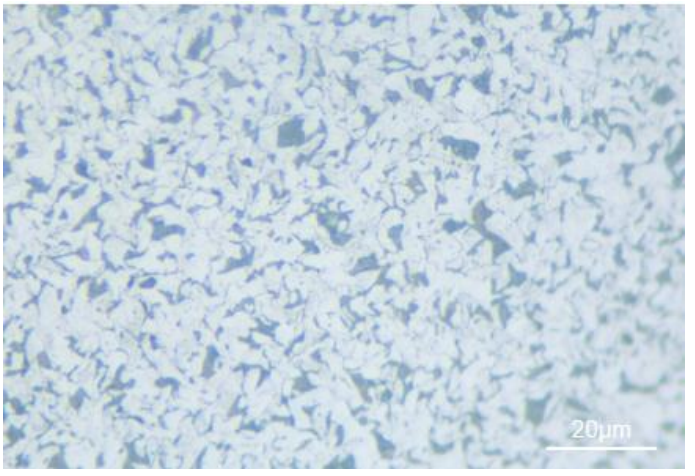

Fig. 1: Metallographic structural diagram of normal steel.

CGL low-carbon steel included ferrite and pearlitic phases. The white areas represent the cubic-lattice-structured ferrite grains. However, the black-and-white lamellar and colorful areas were pearlitic. In this steel, the phase ferrite provided good intensity, plasticity, and resilience. Furthermore, the good grain-boundary state and uniform grain distribution were conducive to the combination of the zinc coating with the matrix. During the galvanizing process, the boundary conditions for Zn atom diffusion and attachment were good. Thus, the zinc coating thickness was uniform, and the bonding strength was high. Finally, the corrosion resistance of the steel improved.

2) Steel metallographic structure after solution corrosion: **Solution** ①: After immersion in the artificial seawater for 5 min, dark spots appeared on the metallographic surface of the sample edge, as shown in Fig. 2(a). These were the corrosion-product-gathering areas of the CGL coating. The seawater ions destroyed the passivation film in the Zn coating, causing corrosive pitting, the dark areas representing the corrosion pits. The overall metallographic structure was relatively stable. However, localized corrosion began to occur.

The metallographic structure of the steel after immersion in the artificial seawater for 24 h is shown in Fig. 2(b). A comparison between Figs. 2(a) and 2(b) reveals that, after 24 h of corrosion, the steel was severely corroded. However, the grain boundaries were unclear. A completely oxidized film was formed. Clean, clear grains and grain boundaries were not apparent. However, under a high-power microscope, it was evident that the corrosion products exhibited a point distribution. They varied in size and were yellow in color but exhibited an uneven distribution, as shown in Fig. 3.

As shown in Fig. 3, even after focusing the microscope, some yellow dots were blurry, whereas others were clear, indicating that they were not at the same level. Some yellow dots started to connect, changing to banding.

Solution ②: After immersion corrosion in the 10% NaCl solution for 5 min, the grain boundaries started to blur. The corrosion areas were larger and more dispersed. The corrosion medium rapidly developed and fully reacted with the steel. After 24 h of immersion corrosion, the grain boundaries and crystal grains were unclear. Corrosion products appeared at the edges of the samples. However, the corrosion reaction did not increase greatly. The surface oxidation film prevented the solution ions from further corroding the steel.

Solution ③: After immersion corrosion in the 3% $NaHCO_3$ solution for 5 min, the grain boundaries and corrosion signs in the grains were not apparent. No corrosive pitting could be observed. The metallographic diagram was essentially the same as the original diagram. After 24 h of immersion corrosion, the metallographic structure remained relatively intact.

Solution ④: After immersion corrosion in the 5% Na_2SO_4 solution for 5 min, the grain boundaries started to blur. The grain boundaries and crystal grains were unclear. Overall, the signs of corrosion were lower. Stray, small pit points and spots appeared. It is likely that the sulfate ions initiated local electrochemical corrosion on the metal surface. However, large-area and concentrated corrosion morphology were not

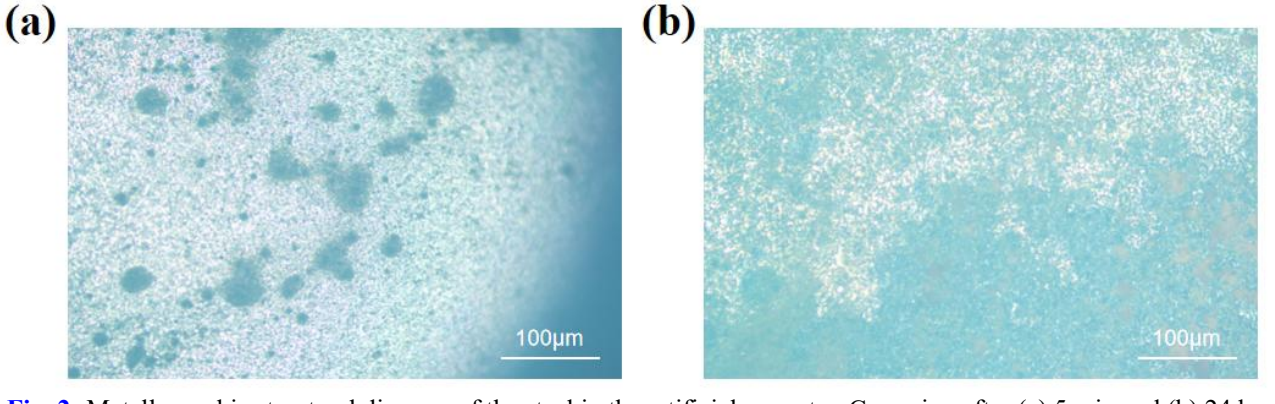

Fig. 2: Metallographic structural diagram of the steel in the artificial seawater. Corrosion after (a) 5 min and (b) 24 h.

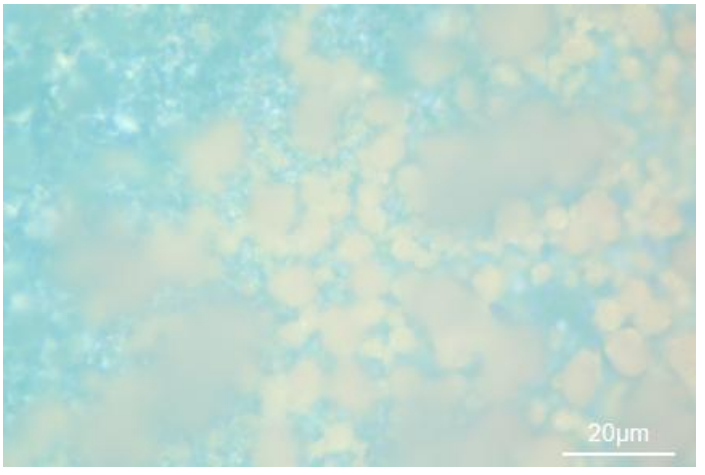

Fig. 3: Structural diagram of the steel corrosion products after artificial seawater immersion for 24 h.

apparent. After 24 h of immersion corrosion, the number of light-colored spots clearly increased and were widely distributed. These spots were interconnected and integrated. It is likely that the initial localized microbattery corrosion gradually developed into a wider electrochemical corrosion area. The corrosion products continuously accumulated on the metal surface.

The metallographic structures of the steel after immersion corrosion in the 5% Na_2SO_4 solution for 5 min and 24 h are shown in Figs. 4(a) and 4(b), respectively. A comparison between Figs. 4(a) and 4(b) shows that the steel corrosion rate during the initial stage was relatively slow. As time progressed, the corrosion rate increased. Compared to the artificial seawater, the steel in the 5% Na_2SO_4 solution corroded considerably until 24 h, indicating that the steel corrosion rate was higher in the artificial seawater over a short period.

Solution ⑤: After immersion corrosion in the 5% $NaHCO_3$ solution for 5 min, the corrosion degree was slight. The grain boundaries and signs of corrosion in the grains were not apparent. No corrosive pitting could be observed. The metallographic diagram was essentially the same as the original diagram. After 24 h of immersion corrosion, the grain boundaries were slightly blurry and a twin-grain boundary appeared.

The metallographic structures of the steel after immersion corrosion in the 5% $NaHCO_3$ solution for 5 min and 24 h are shown in Figs. 5(a) and 5(b). A comparison between Figs. 5(a) and 5(b) shows that during the short corrosion cycle, the degree of steel corrosion was slight and the solution ions did not destroy the internal steel structure.

Solution ⑥: After immersion corrosion in the 5% NaCl solution for 5 min, the grain boundaries and crystal grains were slightly blurred. The twin crystal boundary appeared. After immersion corrosion for 24 h, the ferrite was destroyed. However, no excess corrosion products were observed.

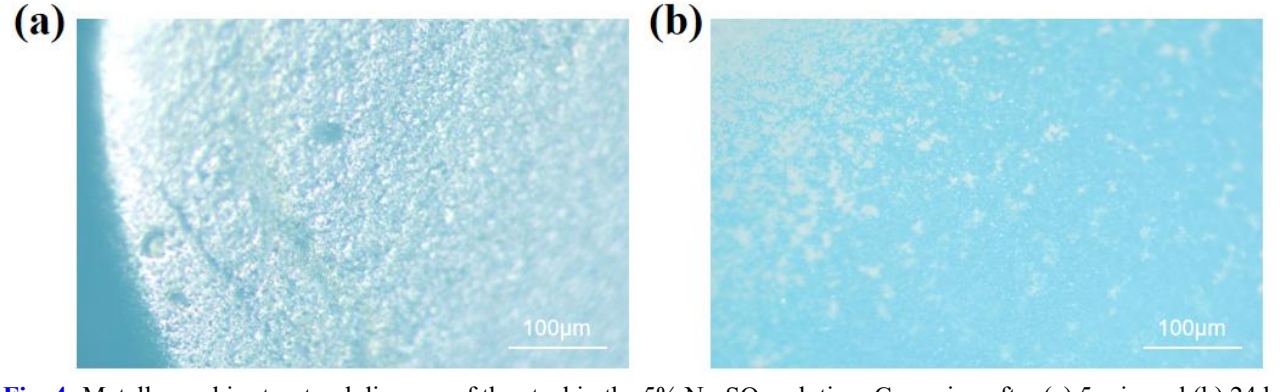

Fig. 4: Metallographic structural diagram of the steel in the 5% Na_2SO_4 solution. Corrosion after (a) 5 min and (b) 24 h.

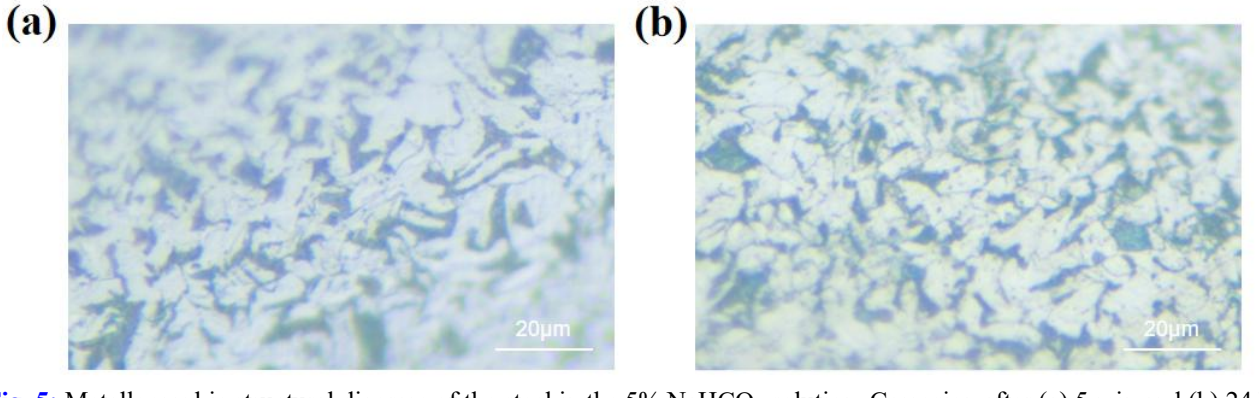

Fig. 5: Metallographic structural diagram of the steel in the 5% $NaHCO_3$ solution. Corrosion after (a) 5 min and (b) 24 h.

3.3 Microscopic experimental result analysis

Based on the above experimental results, the steel samples exhibited grain-boundary blurring in most solutions during early immersion. Corrosion begins, but the corrosion intensities and rates differed. The emergence of the twin crystal boundaries illustrates that the grain boundaries were destroyed. After prolonged immersion times, the grain boundaries and crystal grains were blurry and the steel samples were severely corroded. Furthermore, with the advent of multiple substances, the microscope cannot be completely focused on the multilayered steel surfaces, which causes interface blurring.

Different solutions had different corrosion effects on the CGL low-carbon steel. The strong electrolyte solutions—such as the artificial seawater and NaCl solutions—caused corrosion within a short period of time, with the artificial-seawater corrosiveness being the strongest. During the early corrosion stages, the grain boundaries were blurry. Corrosion pits and tiny spots were also apparent. Over time, the corrosion was aggravated, with the grain boundaries gradually blurring and even disappearing. The crystal grains were destroyed. The corrosion products increased in size and spread. After immersion in the artificial seawater and 10% NaCl solution for 24 h, the grain boundaries and crystal grains were difficult to distinguish. After immersion corrosion in the $NaHC0_3$ solution for 24 h, the metallographic structure was still relatively complete, illustrating that this solution had little effect on corrosion.

As shown in Fig. 6, corrosion began during pitting. The artificial seawater was a medium that typically caused pitting corrosion. After immersion in the corrosion solution for 5 min, dark-colored spotted corrosion pits appeared on the metallographic surfaces of the samples, owing to the chloride ions in the artificial seawater destroying the passivation film of the zinc coating. After immersion corrosion for 24 h, the spots were connected over a large area, indicative of changes in the corrosion morphology.

3.4 Electrochemical workstation test results and analysis

1) Open-circuit potential: As presented in Table 9, the open-circuit potential values in the different solutions were in the following order: Solution ② > Solution ① > Solution ③ > Solution ④, illustrating that the CGL steel wire was easily corroded in solutions that included Cl^- ions. Conversely, in the HCO_3^- solution, the CGL steel wire exhibited little corrosion.

2) Resistance test: From the resistance Nyquist pattern test results, the internal resistance values in the different solutions were in the following order: Solution ④ > Solution ③ > Solution ② > Solution ①. The internal resistance in Solution ④ was much higher than that in the other solutions. The internal resistances in Solutions ② and ① exhibited a small gap, illustrating that the CGL steel was barely corroded in the solution including HCO_3^- ions. However, in the artificial seawater, the steel was severely corroded. Based on the highest-frequency scan points, the arc diameter of the Nyquist patterns for all solutions could be calculated. The arc diameter sizes in the different solutions were in the following order: Solution ④ > Solution ③ > Solution ② > Solution ①. The larger the arc diameter, the lower the degree of steel corrosion in the solution.

3) Polarization curve test: As shown in Fig. 7, the CGL steel wire was deactivated in the corrosion solution. The current was either maintained at a constant level or changed slowly, forming a broken line. The surface of the material produced oxides that protected the internal steel. When the electric potential was sufficiently high, the oxides

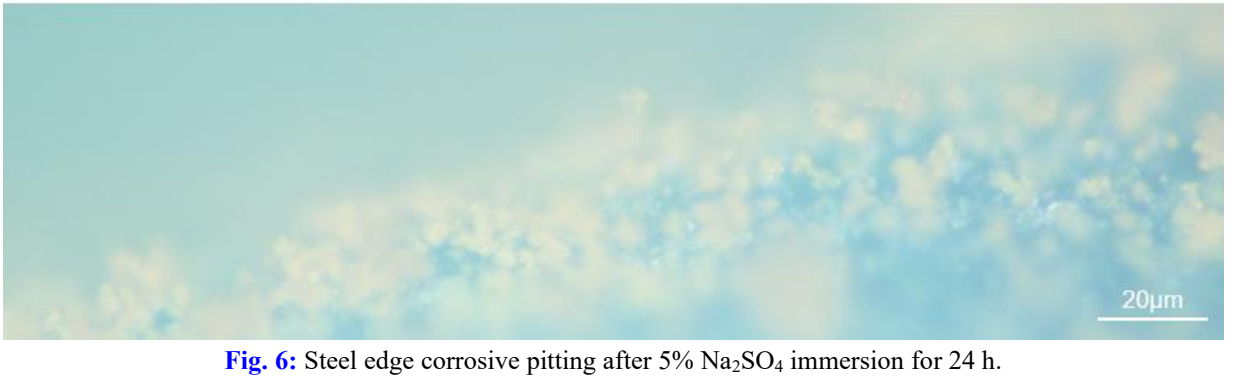

Fig. 6: Steel edge corrosive pitting after 5% Na_2SO_4 immersion for 24 h.

Table 9: Open-circuit potential values in different solutions.

Solution	①	②	③	④
E_{OCP} (V)	−1.069	−1.041	−1.218	−1.226

disintegrated. The electric current changed with the electric potential. Based on the polarization curve calculations, the current densities could be obtained as follows: Solution ① > Solution ② > Solution ③ > Solution ④. When passivation was complete, the steel could not be protected by the oxidation film and the internal steel underwent accelerated corrosion. The steel corrosion rate was fastest in the artificial seawater.

The test results in Fig. 7 show that all the corrosion potentials were negative. In the different solutions, the corrosion potential values were in the following order: Solution ② > Solution ① > Solution ③ > Solution ④. Because the cathodic protection could be represented by the corrosion potential, it was difficult to corrode the steel oxidation film formed in Solution ④. However, in Solution ②, the steel was easily corroded. This was slightly different from the test results described above. Considering the error effects and corrosion behavior evaluation mechanisms, the final conclusion was subject to the current density test results.

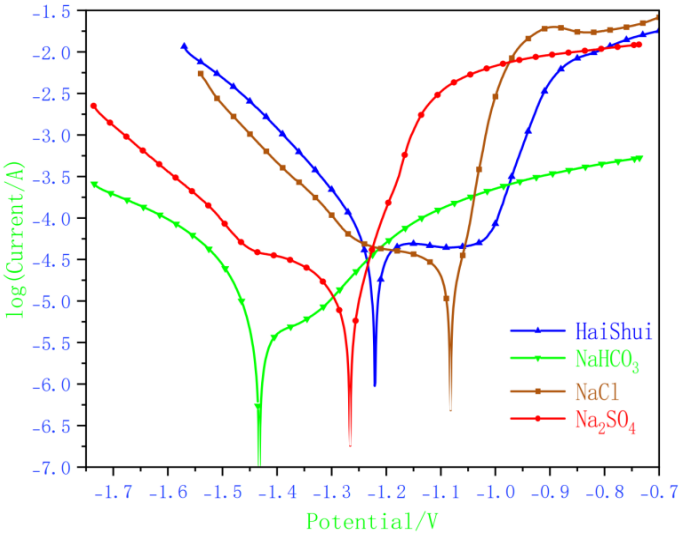

Fig. 7: Polarization voltammogram in the different solutions.

4. Conclusion

In this study, the corrosion resistance of submarine cable steel armor was explored using immersion corrosion detection and electrochemical workstation tests. Control groups were used in these experiments. The corrosion of the steel samples was accelerated using a high-concentration corrosion solution. In addition to the macroscopic examination, the steel metallographic microstructure was examined using a metallurgical microscope. Additionally, electrochemical measurement technology was used to test the open-circuit potential, electrochemical impedance spectroscopy (EIS), and polarization curves. Based on the metallographic structure examination, the macroscopic and microscopic features of the steel surface before and after corrosion could be visually presented. In the open-circuit potential test, the corrosion tendency of the submarine cable steel armor with different seawater factors could be estimated. In the EIS test, the degree of steel corrosion in different solutions could be obtained based on an analysis of the impedance characteristics at different frequencies. In the polarization curve test, the steel polarization behavior and corrosion mechanism in different solutions could be explored, based on corrosion potential and current density analysis. From the test results, different solutions exhibited different corrosion effects on the steel armor. This was because the negative ion types, content, and concentrations differed. In low-salinity, shallow-water areas, the steel corrosion rate is relatively low, primarily because there are fewer ions (such as Cl^-) corroding the steel in such environments, making it difficult for the electrochemical reactions required to accelerate steel corrosion to occur. In deep sea, there are more corrosive ions (such as SO_4^{2-} and Cl^-) and the steel corrosion rate is high. With an increase in these negative ions, the corrosion rate also increases. Based on the experimental results, the corrosion rate of the CGL steel wire was limited to the initial corrosion stages. Passivation occurred during the electrochemical reactions, owing to the oxidation or passivation film that formed on the surface of the zinc coating, which prevented the further corrosion of the steel wires. If steel with higher corrosion resistance is required in the future, special coatings or materials could be added to the steel surface. A new type of armor-layer material should be able to fulfill the different seawater environmental requirements.

Acknowledgments

This research was aided by the key area campaign of regular universities in Guangdong province (Nos. 2021ZDZX1058 and 2024ZDZX4074), Guangdong Basic and Applied Basic Research Foundation (Nos. 2025A1515010595 and 2023A1515240063).

Conflict of Interest

There is no conflict of interest.

Supporting Information

Applicable.

CRediT Statement

Guang Yu: Writing – review & editing, Supervision, Resources, Project administration, Investigation, Supervision, Software. **Lijie Peng:** Writing – Original draft, Methodology, Investigation, Formal analysis, Data curation. **Yujia Cheng**: Writing – review & editing, Funding acquisition. Pengcheng

Wang: Supervision, Resources.

References

[1] T. Zhang, Z. Fan, N. Ning, J. Tang, D. Kou, Analysis of engineering and geological conditions of international submarine optical fiber cable routing in the East China Sea section, *Geofluids*, 2022, **2022**, 2527979, doi: 10.1155/2022/2527979.

[2] M. B. Hossain, M. R. Islam, K. M. Muttaqi, D. Sutanto, A. P. Agalgaonkar, A power dispatch allocation strategy to produce green hydrogen in a grid-integrated offshore hybrid energy system, *International Journal of Hydrogen Energy*, 2024, **62**, 1103-1112, doi: 10.1016/j.ijhydene.2024.03.051.

[3] K. Chae, W. Nam, C. Shim, Influence of coiling behavior on axial stress in steel wires of submarine power cables: a numerical study, *Ocean Engineering*, 2023, **288**, 116014, doi: 10.1016/j.oceaneng.2023.116014.

[4] H. Huang, Q. Zhang, H. Xu, Z. Li, X. Tian, S. Fang, J. Zheng, E. Zhang, D. Yang, Risk identification and safety evaluation of offshore wind power submarine cable construction, *Journal of Marine Science and Engineering*, 2024, **12**, 1718, doi: 10.3390/jmse12101718.

[5] C. Cao, W. Hao, Y. Ge, J. Chen, W. Wang, C. Xu, Shape monitoring method of submarine cable based on fiber Bragg grating, *Optical Fiber Technology*, 2023, **77**, 103255, doi: 10.1016/j.yofte.2023.103255.

[6] J. Shu, Q. Wang, W. Zhang, M. Du, J. Lin, Passive acoustic localization of submarine cable breakdowns using MUSIC algorithm combined with deep learning, *Marine Geophysical Research*, 2025, **46**, 5, doi: 10.1007/s11001-025-09567-6.

[7] P. Li, Y. Chen, H. Huang, H. Zhang, H. Xie, H. Piao, Investigation of corrosion behavior of galvanized steel as submarine cable armor in seawater under weak magnetic fields, *International Journal of Electrochemical Science*, 2023, **18**, 100264, doi: 10.1016/j.ijoes.2023.100264.

[8] Z. Jiang, S. Dong, Y. Zhang, G. Liu, T. Dong, Corrosion of copper armor caused by induced current in a 500 kV alternating current submarine cable, *Electric Power Systems Research*, 2021, **195**, 107144, doi: 10.1016/j.epsr.2021.107144.

[9] R. Guo, P. Yang, F. Mao, J. Li, L. Chen, G. Yu, D. MacDonald, Electrochemical noise studies on complex galvanic corrosion of submarine cable armor layer in artificial seawater, *Materials and Corrosion*, 2022, **73**, 379-392, doi: 10.1002/maco.202112803.

[10] Z. Lu, C. Cao, Y. Ge, J. He, Z. Yu, J. Chen, X. Zheng, Research on improving the working efficiency of hydraulic jet submarine cable laying machine, *Journal of Marine Science and Engineering*, 2021, **9**, 745, doi: 10.3390/jmse9070745.

[11] Y. Liang, Y. Du, Z. Zhu, L. Chen, Y. Liu, L. Zhang, L. Qiao, Investigation on AC corrosion of aluminum alloy sacrificial anode in the artificial simulated seawater environment, *Electrochimica Acta*, 2023, **446**, 142002, doi: 10.1016/j.electacta.2023.142002.

[12] X. Zhao, R. Liu, W. Qi, Y. Yang, Corrosion resistance of concrete reinforced by zinc phosphate pretreated steel fiber in the presence of chloride ions, *Materials*, 2020, **13**, 3636, doi: 10.3390/ma13163636.

[13] P. Li, Y. Chen, H. Huang, H. Zhang, H. Xie, H.-G. Piao, Investigation of corrosion behavior of galvanized steel as submarine cable armor in seawater under weak magnetic fields, *International Journal of Electrochemical Science*, 2023, **18**, 100264, doi: 10.1016/j.ijoes.2023.100264.

[14] R. Guo, P. Yang, F. Mao, J. Li, L. Chen, G. Yu, D. MacDonald, Electrochemical noise studies on complex galvanic corrosion of submarine cable armor layer in artificial seawater, *Materials and Corrosion*, 2022, **73**, 379-392, doi: 10.1002/maco.202112803.

[15] A. M. Kumar, I. U. H. Toor, Dynamic and localized microelectrochemical approaches to evaluate the corrosion resistance of newly developed lean duplex stainless steel alloys, *Materials and Corrosion*, 2022, **73**, 1687-1700, doi: 10.1002/maco.202213174.

[16] E. Seixas Campos, J. da Silva de Sá, T. Seixas Campos, E. Alencar de Souza, J. A. da Cunha Ponciano Gomes, Influence of metallurgical factors on the hydrogen induced cracking of carbon steel wires in H_2S-containing environments, *Engineering Failure Analysis*, 2024, **155**, 107739, doi: 10.1016/j.engfailanal.2023.107739.

[17] D. Qiao, S. Wang, P. Ning, Q. Liu, N. Chen, J. Wang, J. Chen, X. Zhang, K. Xiao, Corrosion resistance of zinc-magnesium-aluminium alloy coated steel in marine atmospheric environments, *International Journal of Electrochemical Science*, 2024, **19**, 100705, doi: 10.1016/j.ijoes.2024.100705.

[18] M. A. Deyab, Q. Mohsen, Development of tailor-made ionic liquid to resist corrosion in the heat exchanger of a multistage flash (MSF) desalination system, *Desalination*, 2025, **614**, 119147, doi: 10.1016/j.desal.2025.119147.

[19] E. Barmatov, J. Stoney, J. Staniland, T. Hughes, Z. Qian, S. P. Putra, M. Gummadi, A. Hendrawinata, A. Medvedev, Corrosion of galvanized armor wires under simulated wellbore and atmospheric conditions, *Corrosion Science*, 2025, **253**, 112997, doi: 10.1016/j.corsci.2025.112997.

[20] F. Cruz, I. Valente, J. Almeida, A. Neves, E. Pereira, Experimental characterization of bond between concrete and HDG steel tubes for mixed steel-concrete structures, *Materials and Structures*, 2024, **57**, 89, doi: 10.1617/s11527-024-02352-8.

[21] A. Ashfaq, U. Khalique, A. Nadeem, A. A. Rizvi, Comprehensive analysis of temperature distribution in OPGW cable considering ramifications of short circuit current, *Scientific Reports*, 2025, **15**, 21949, doi: 10.1038/s41598-025-09266-7.

[22] S. Xue, R. Shen, Tensile–bending–corrosion fatigue analysis of the parallel steel wire cable in suspension bridges, *Journal of Bridge Engineering*, 2024, **29**, 04024007, doi: 10.1061/jbenf2.beeng-6621.